Journal of Materials Chemistry A

ROYAL SOCIETY OF CHEMISTRY

PAPER

View Article Online
View Journal | View Issue

Cite this: J. Mater. Chem. A, 2024, 12, 18469

Investigation of sodium insertion in hard carbon with *operando* small angle neutron scattering†

Emily M. Reynolds, [ab] Jack Fitzpatrick,[ac] Martin O. Jones,[ab] Nuria Tapia-Ruiz,[ac] Helen Y. Playford, [ab] Stephen Hull,[ab] Innes McClelland, [ad] Peter J. Baker, [ab] Serena A. Cussen ‡[ad] and Gabriel E. Pérez *[ab]

Received 8th August 2023
Accepted 23rd June 2024

DOI: 10.1039/d3ta04739c

rsc.li/materials-a

Sodium-ion battery technology is a promising and more sustainable alternative to its more conventional lithium-ion based counterpart. The most common anode material for these systems is a disordered form of graphite known as hard carbon. The inherent disorder in these carbons results in multiple possible pathways for sodium storage making the characterisation of sodiation mechanisms during cycling highly challenging. Here, we report an *operando* small angle neutron scattering (SANS) investigation of sodiation in a commercial hard carbon using a custom electrochemical cell. We demonstrate that it is possible to discern different sodiation mechanisms throughout cycling and provide supporting evidence for a three-stage model in which sodium ions are first adsorbed onto the surface of particles, then intercalated into the graphene layers, and finally inserted into the nanopores during the electrochemical stage known as the plateau region. This study showcases the unique capabilities of *operando* SANS for the characterisation of sodiation mechanisms of carbon-based, disordered, porous materials.

1 Introduction

Hard carbon (HC) is a class of disordered carbonaceous material that has been extensively investigated as an anode material for sodium-ion batteries (SIBs).[1–3] Hard carbons have high specific capacities ranging from 200–500 mA h g^{-1}, excellent cycling stability, low operating voltages *vs.* Na^+/Na, and can be produced by facile synthesis procedures from widely available biological precursors. Whilst the charge storage mechanisms of hard carbon have been extensively studied, their characterisation is notoriously challenging and a fundamental understanding of this process remains elusive. This is essential to guide development towards materials with competitive electrochemical properties, and for enabling the tunning of electrochemical properties such as power and capacity to specific applications.

HC is produced *via* high-temperature pyrolysis (generally between 800–2000 °C) of organic precursors such as lignin and sucrose, whose highly branched and crosslinked nature prevents complete graphitisation.[4,5] The structure of HCs consists of randomly orientated local domains of stacked graphene sheets of varying curvature, which are disrupted by highly disordered regions that arise as a consequence of defects, vacancies, and the presence of heteroatoms. The defects and resulting curvature increase the interlayer spacing relative to graphite, and the mismatch of ordered and disordered domains causes closed pores to form within the bulk of the material. This structure has been previously described by the widely accepted "house of cards" model developed by Dahn *et al.*[6–8] A typical galvanostatic discharge/charge profile of HC consists of two potential regions: a sloping region at potentials above 0.1 V and a plateau region at potentials below 0.1 V where there is significant capacity gain over almost constant potential. These regions are thought to correspond to distinct sodium storage processes, but the specific assignment of these processes is highly debated in literature.

The variety and complexity of HC structures is partly responsible for the challenge of understanding their sodium storage mechanism. The Na^+ ions can be stored through multiple pathways in the highly disordered structure of HCs[4,9] including intercalation between the graphene sheets within the ordered graphitic domains, the adsorption at reactive surface sites (*e.g.* vacancies and dangling bonds at the edges of the graphitic domains) and the filling of the closed pores. Stevens and Dahn were the first to suggest a sodium storage model with

[a]The Faraday Institution, Harwell Science and Innovation Campus, OX11 0RA, UK. E-mail: gabriel.perez@stfc.ac.uk

[b]ISIS Neutron and Muon Source, Rutherford Appleton Laboratory, Harwell Science and Innovation Campus, OX11 0QX, UK

[c]Department of Chemistry, Molecular Sciences Research Hub, Imperial College London, White City Campus, London, W12 0BZ, UK

[d]Department of Materials Science and Engineering, The University of Sheffield, Sheffield, S10 2TN, UK

† Electronic supplementary information (ESI) available. See DOI: https://doi.org/10.1039/d3ta04739c

‡ Present address: School of Chemistry, University College Dublin, Belfield, Dublin 4, Ireland

a two-stage "intercalation-pore filling" model derived from *in situ* small and wide angle X-ray scattering (SAXS and WAXS respectively) studies of glucose-derived HCs.[10–12] They attributed the sloping region to the intercalation of sodium between the graphene sheets, and the plateau region to the insertion of sodium into the closed pores.

Assignment of the plateau region to either or both intercalation and pore-filling processes is still a point of discussion, with evidence for intercalation mainly based on the observation of an expansion in the graphitic interlayer distance at potentials within the plateau region from *ex situ* X-ray diffraction (XRD) measurements.[13,14] Additionally, changes in the plateau capacity of HC produced at various temperatures can be correlated to changes in the calculated interlayer spacing.[14–18] Meanwhile pore-filling has been supported through the correlation of closed pore volumes to the plateau capacity of various HCs, as well as *operando* NMR and Raman studies.[19] This has resulted in the proposal of at least three more sodium storage models, "adsorption-intercalation", "adsorption-filling" and a "three-stage" model in which the low potential plateau region is split between intercalation and pore-filling processes.[15,20,21] Understanding the extent to which intercalation and pore-filling contribute to the plateau region of HCs is of great interest, as a complete understanding of sodium storage in HCs will allow their tailoring for specific electrochemical properties.

One of the main reasons behind the discrepancies in understanding the sodiation mechanisms of HC at different points during cycling is the limitations of the characterisation techniques used to conduct such investigations. Small angle neutron scattering (SANS) is a non-destructive, highly penetrating, and sample-average characterisation technique capable of probing both the open (surface) and closed (bulk) porosity of HC.[22,23] Moreover, the neutron scattering length of sodium is nearly half of carbon's providing a considerably different contrast to that obtained with X-rays. This can allow the clearer elucidation of sodiation mechanisms in hard carbon. SANS data from HCs show a slope at low Q (below 0.04 Å^{-1}) which is attributed to surface scattering of the individual particles and a shoulder at higher $Q \sim 0.1$ Å^{-1} resulting from the scattering of the pores within the bulk of the hard carbon.[24] Whilst the peak position of this shoulder corresponds to the average distance between the pores, its intensity is proportional to the scattering length density (SLD) contrast between the bulk carbon matrix and the content of the pores. Therefore, it is possible to study the mechanism of sodium insertion during discharge by tracking the changes in the shoulder during cycling as the processes of intercalation and pore-filling will yield different SLD contrasts (Fig. 1b).

In this study, an *operando* SANS experiment was conducted using a custom-built Na-ion half cell to elucidate the mechanisms of sodiation of HC during discharge. While *ex situ* SANS measurements have been used to understand the structure of HCs, and an *in situ* SAXS experiment on the sodiation of a HC has been reported, we report the first *operando* SANS experiment, to the best of our knowledge, to investigate this process. The *operando* nature of this study enabled the deconvolution and direct observation of intercalation and pore-filling processes occurring at specific voltage ranges within the commercial hard carbon during initial discharge.

2 Experimental

2.1 Hard carbon

The commercial hard carbon used for this study was a Kuranode type 1 (Kuraray Co. Ltd), which the supplier reports can achieve capacities up to 280 mA h g^{-1} *vs.* Na and is reported to have a specific surface area of 4 m^2 g^{-1}.[25] The morphological characteristics of this hard carbon as reported by the supplier were corroborated with SAXS, which was also used to determine the average pore size (Fig. S1†).

2.2 Electrochemistry

We used a bespoke electrochemical cell made at ISIS for *operando* studies of battery materials (Fig. S2†).[26] The cell has a coin cell geometry that is compatible with small-angle scattering instruments that measure in transmission mode, and an appropriate window size to obtain good time-resolved data for typical neutron count rates on the SANS-I instrument at SINQ. The cell uses 0.2 mm thick aluminium sheets as current collectors, a 0.5 mm fluorosilicate gasket, and a stainless steel outer casing. Hard carbon was mixed with 3 wt% carboxymethyl cellulose sodium salt binder (MW 250000, Thermo Scientific™) and water using a Thinky mixer to create a slurry, before being cast on the aluminium current collector to obtain a thickness of 0.7 mm and covering a circular area of 1 cm^2 to match the beam aperture. The coating was dried under vacuum at 100 °C overnight in a vacuum oven. The cell was assembled in an MBraun Argon glovebox (O_2 and H_2O <0.1 ppm) using a glass fiber filter (Whatman) as the separator, 150 µl $NaPF_6$ in EC/DEC (1 : 1 v/v) (Kishida) of electrolyte, and a 1 mm thick disc with a diameter of 16 mm of rolled sodium metal (99.8% oiled sticks, Thermo Scientific™). A copper washer was added between the current collector in which the HC was cast and the stainless steel casing to increase the pressure within the cell and the cell was sealed using 8 PEEK screws. Galvanostatic charge/discharge sequences were carried out using a Biologic VSP-300 in the potential window 0.01–2.5 V *vs.* Na^+/Na at a rate of C/20 (the current was calculated assuming a practical capacity of 200 mA h g^{-1}) after a 10 h rest period for the offline tests, and a 30 minute rest period for the test in the beam.

2.3 *Operando* SANS

SANS measurements were carried out on the SANS-I instrument at the SINQ facility in the Paul Scherrer Institut in Switzerland.[27] The wavelength used was $\lambda = 5$ Å and the sample to detector distance was 1.52 m with a collimation of 6 m. These settings resulted in a total covered Q range of 0.01 Å$^{-1} \leq Q \leq 0.7$ Å^{-1}. The *operando* cell depicted in Fig. S2† has a nominal active area of 1.5 cm^2 designed for a circular beam. A circular cadmium shield with a 16 mm diameter aperture was secured to the front of the cell to aid alignment and to define the active area in the beam. Continuous time-dependent SANS measurements were collected as the cell was discharged and the data were sliced into profiles corresponding to a two-minute collection time,

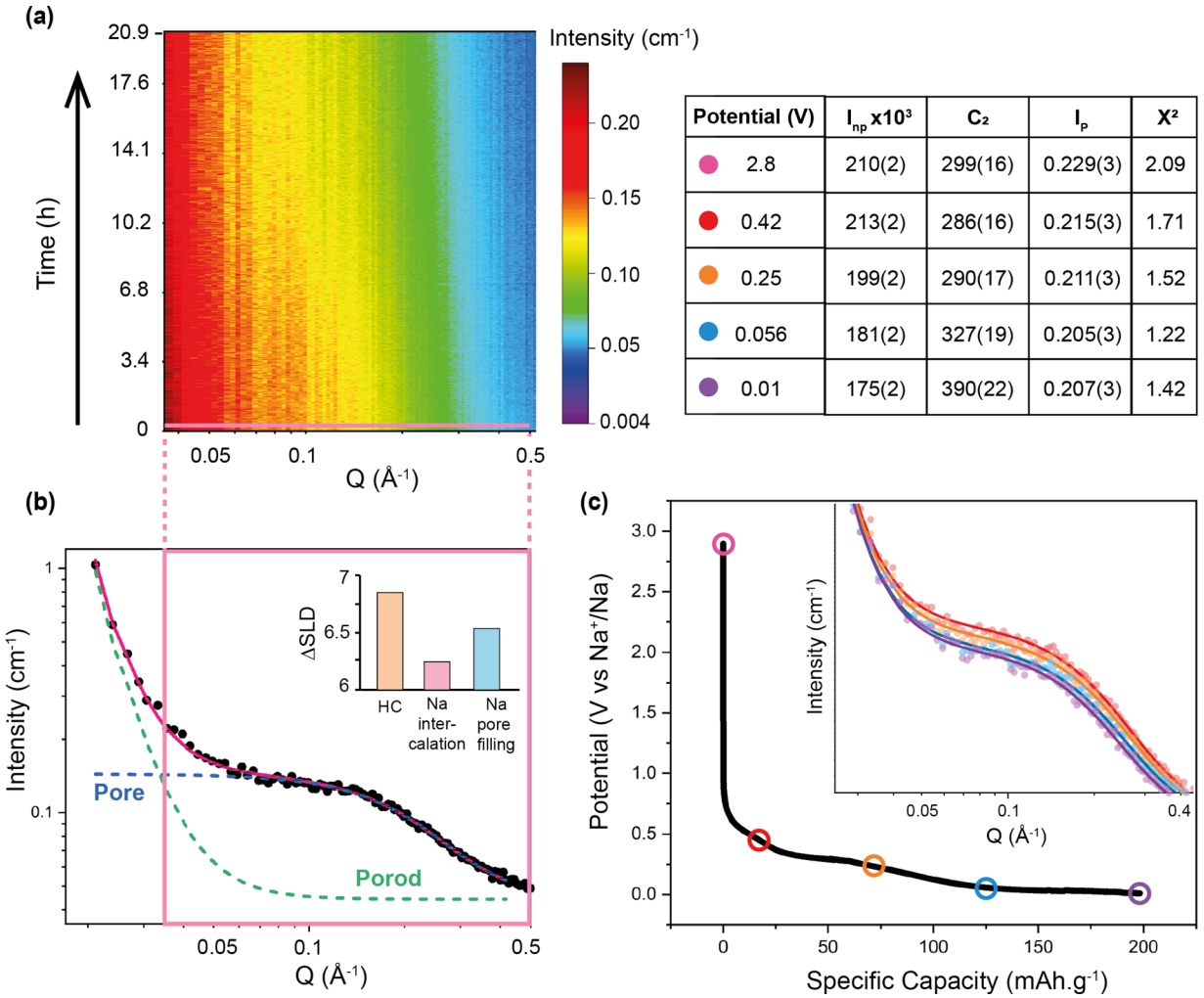

Potential (V)	I_{np} x10³	C_2	I_p	X^2
2.8	210(2)	299(16)	0.229(3)	2.09
0.42	213(2)	286(16)	0.215(3)	1.71
0.25	199(2)	290(17)	0.211(3)	1.52
0.056	181(2)	327(19)	0.205(3)	1.22
0.01	175(2)	390(22)	0.207(3)	1.42

Fig. 1 (a) Contour plot showing the SANS intensity change of the nanopore feature as a function of time during discharge at a C/20 rate. (b) A single SANS profile (black symbols) collected at 2.7 V with it's corresponding fit (dark pink) of the Teubner–Strey model (shown as its two main components separately in blue and green). The inset shows the calculated ΔSLD of the HC before sodiation (orange) compared to the HC with Na intercalated in the graphitic domains (pink) and Na in the pores (teal). (c) The electrochemical discharge curve obtained during the *operando* experiment with an inset showing SANS data collected at different discharge points with the data shown as symbols and the corresponding fits as lines. Note that the pink profile is not visible as it is identical to the next one in red. The table shows values obtained from fitting the selected patterns in (c).

each. The beam passed through two 0.2 mm Al current collectors, the 1 mm thick Na metal counter electrode, the 0.5 mm hard carbon electrode, and the glass fibre separator soaked in electrolyte. A measurement of the empty cell with everything in it except the hard carbon was collected and used to subtract the scattering from all the components that were not of interest from each profile during the normalisation of the data to obtain absolute intensity units. The 1D profiles were obtained by averaging the 2D scattering data using the Grasp Lockdown software, which was also used for the normalisation of the data. SANS patterns were modelled using the SASView software.

3 Results and discussion

3.1 SANS model

To investigate sodium insertion into the hard carbon pores during discharge, we tracked the change in the SANS intensity. The intensity is proportional to the square of the difference between the scattering length density values of the hard carbon and the pores, ΔSLD^2. The SLD is dependent on the chemical composition of the scattering object and thus will change for the carbon network and the pores as sodium is incorporated into them. To quantify the relative change of the SANS intensity, we fitted each SANS profile to a Teubner–Strey model which describes a two-phase system that has similar volume fractions and an average distance, d, between domains of the same phase.[22] This is comparable to the nanopore structure of hard carbon, which can be considered as a totally disordered two-phase system, making the Teubner–Strey model equivalent to the well-known Debye–Bueche model for totally random two-phase systems.

$$I(Q) = B + \frac{I_{\text{Porod}}}{Q^p} + \frac{I_{\text{nanopore}}}{1 + C_1 Q^2 + C_2 Q^4} \quad (1)$$

The SANS data are fit using eqn (1) – a combination of a modified Porod expression for the low Q scattering from the particle surface (green dashed line in Fig. 1b) and the semi-empirical model for the nanopore feature (blue dashed line in Fig. 1b). In this equation, B is a background term, I_{Porod} and I_{nanopore} are scale terms for the Porod and nanopore functions, respectively, p is the Porod exponent, and C_1 and C_2 are adjustable parameters described in the ESI.† The low Q region shows the expected Q^{-4} dependency ($p = 4$ in eqn (1)), which is due to the size of the grains relative to the observed Q range. Fig. 1b shows an excellent fit of the model (separated into its two main compoments) to data from the cell before discharge. As shown in eqn (S1)† the scale term I_{nanopore} from the pore component is proportional to the square of the scattering length density contrast (ΔSLD^2) between the pores and the carbon framework. By following the change in this parameter with cycling, we were able to extract information about the change in the composition of the pores and carbon framework.

3.2 *Operando* SANS

The electrochemical behaviour of the cell during charge and discharge during the first three cycles was tested offline (Fig S3†). A first cycle discharge and charge capacity of 163 mA h g^{-1} and 134 mA h g^{-1}, respectively, were obtained resulting in an initial coulombic efficiency (ICE) of 82%. The sloping (>0.1 V) and plateau (<0.1 V) regions as reported in the literature are clearly observed in the discharge profiles. During the *operando* SANS experiment, a full initial discharge (sodiation) of the cell achieved a capacity of 197 mA h g^{-1} (Fig. 1c), where both the sloping and plateau regions were also visible. As measurements were taken during the first discharge, we expect the formation of a solid electrolyte interface (SEI). From the offline electrochemical testing, we have estimated that the SEI formation can account for up to approximately 18% (35 mA h g^{-1}) of the first discharge capacity that is irreversibly lost in subsequent cycles. This also accounts for the extra humps at 0.5 V and 0.3 V in the first discharge profile which are only observed during the initial discharge as shown in Fig. S3.† The corrected SANS profiles (background subtracted) are shown as a contour plot in Fig. 1. In total, there were 574 neutron profiles collected in the 20 hours of cell discharge. The nanopore feature is visible (Fig. 1b) and, as expected, decreases in intensity during the discharge as a result of the change in SLD contrast between the carbon and the contents of the pores upon sodiation (Fig. 1c).

Using the model described above we obtain an excellent fit to all the SANS profiles (Fig. 1b and S4†) with a resulting χ^2 value of no more than 2.1%. Selected fitted SANS patterns and details of these fits are shown in the inset of Fig. 1c and the table, and are also included in the ESI.† From the fitted data extracted the I_{nanopore} term, which is proportional to the square of the SLD contrast (ΔSLD^2, extracted from eqn S1†) between the content of the pores and the carbon framework. Fig. 2 shows ΔSLD^2 obtained from I_{nanopore} as a function of time during discharge, overlayed with the discharge profile. Upon immediate inspection of the change of ΔSLD^2 as a function of discharge, three clear different regions are identified. These are highlighted in the discharge profile of the cell in Fig. 2.

In the first region from 0–3.38 h (0–30 mA h g^{-1}, 2.8–0.325 V) we see a relatively steep slope in the discharge profile. There is initially no change in ΔSLD^2 within error, and then a small increase is observed. The small number of points and large error, relative to the change in ΔSLD^2 observed, make it difficult to interpret this as a real change. It is clear, however, that within the first region, there is certainly not a decrease in ΔSLD^2. This indicates that there isn't any Na entering the hard carbon material within the graphitic domains or the closed pores as this would cause a decrease in SANS intensity (see SLD calculations section in the ESI†). Therefore, we assign this capacity to both adsorption of Na ions on the surface of the HC particles and the beginning of SEI formation, although we are unable to distinguish between these processes. This observation is in contrast to suggestions that the first region is associated with Na intercalation into defects within the graphitic layers.[28]

The second region, occurring between 3.38–12.33 h (34–120 mA h g^{-1}, 0.325–0.0653 V), exhibits a much larger decrease in ΔSLD^2 than the third region, occurring between 12.33–20 h (120.6–197 mA h g^{-1}, 0.065–0.01 V), as evidenced by the slopes (-0.0150 ± 0.0003 and -0.0046 ± 0.0004, respectively). To explain this observation, we considered the effects of Na intercalation and pore filling on the ΔSLD^2. We would expect Na intercalation between the graphitic interlayers of the carbon framework to cause the ΔSLD^2 to decrease. This is because Na has a smaller scattering length than carbon, and thus the insertion of sodium into the carbon framework will cause the SLD of the carbon framework to decrease relative to the pristine material, resulting in an overall smaller SLD contrast between the carbon framework and the pores (Fig. 1b). We would also expect an overall decrease in ΔSLD^2 for pore filling, as Na present in the pores would increase the SLD of the pores but would not affect the SLD of the carbon network. However, based on our SLD contrast calculations (ESI Table 1†), we expect the decrease in SLD contrast to be larger for Na intercalation than for pore-filling, these relative differences are shown in the inset to Fig. 1b. Therefore the observed difference in the rate of change of ΔSLD^2 between regions 2 and 3 may be explained by the tentative assignment of region 2 to Na intercalation and region 3 to filling of the closed pores with Na. Nyquist plots from electrochemical impedance spectroscopy measurements taken at various point during discharge (Fig. S5†) show a consistent trend with decreasing voltage up until 0.1 V, from which the trend is reversed with further decreasing voltage. A quantitative analysis of the data in such a complex system is beyond the scope of this study; however the reversing of the trend suggests a major change in the electrochemical processes within the system. This occurs during the voltages at which pore filling is expected which could further support the starting of such stage.

3.3 SLD calculations

In order to model these processes, we performed theoretical calculations of the expected change in ΔSLD^2. Dilatometry

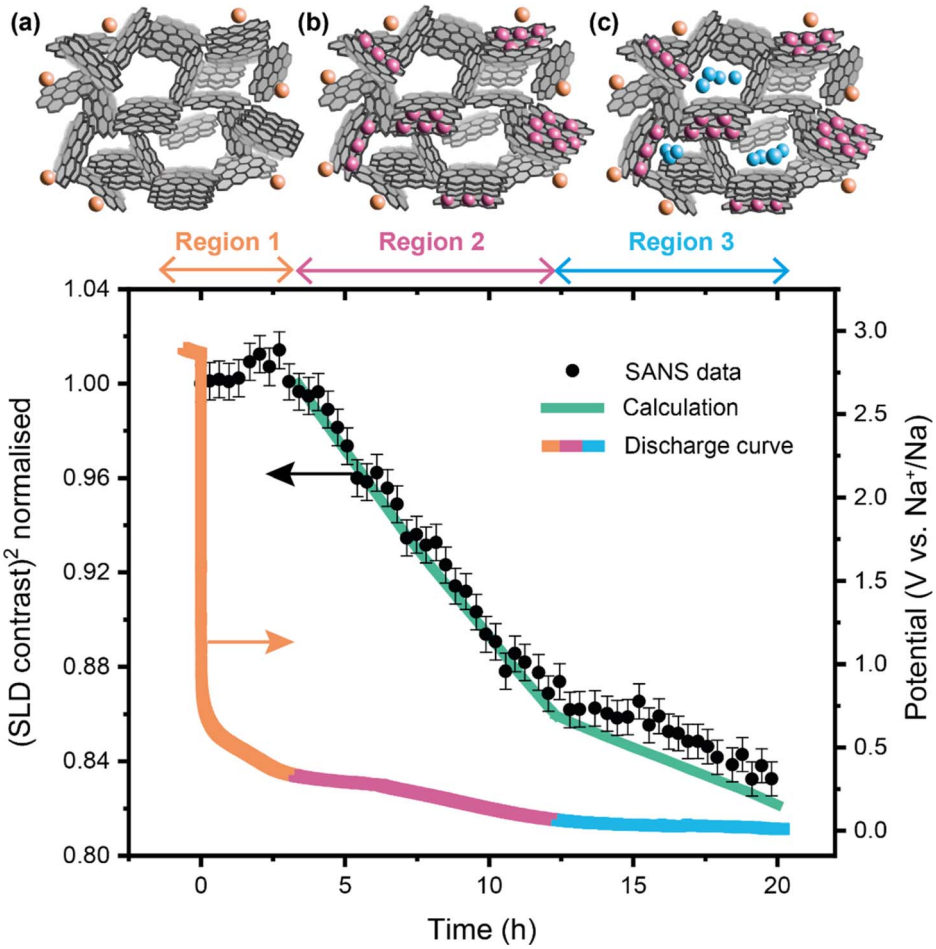

Fig. 2 ΔSLD^2 extracted from fitting the SANS data (black circles) as a function of time during discharge, with the ΔSLD^2 obtained from theoretical calculations overlayed (green line). The electrochemical discharge profile is also presented, with colours corresponding to the different regions observed in the ΔSLD^2 data and different sodiation mechanisms represented in the HC images – (a) surface/SEI formation (orange), (b) intercalation into graphitic regions (pink), and (c) pore filling (blue).

measurements reported elsewhere[29] were used to estimate the density change of the sodiated carbon and electrolyte, and we calculated the SLD of sodiated electrolyte assuming that it is ionic sodium entering into the pores. Our calculations of the change in ΔSLD^2 expected from intercalation are consistent with the observed values, shown in Fig. 2, allowing for a more confident assignment of the second region to Na intercalation into the graphitic regions of the carbon framework. For the third region, our calculations assuming Na enters the pores have the same slope as the experimentally obtained ΔSLD^2 (-0.00422 ± 0.00005), however, they slightly overestimate the ΔSLD^2 values. This discrepancy could be due to the formation of Na metal clusters in the pores during the plateau region,[2] which are not accounted for in our calculations. Regardless of this, this analysis supports assigning this final region to pore filling.

Our results are broadly consistent with the findings of Dahn *et al.* who carried out an *in situ* SAXS experiment on the sodiation of hard carbon using laboratory X-rays and a C-rate of C/90.[12] The discharge profile reported had a different shape to ours which makes direct comparison difficult; this could be due to the slower C-rate used or the type of carbon used (pyrolyzed glucose). Nevertheless, they observed a decrease in intensity during their plateau region which they assigned to pore-filling with calculations similar to those described above. However, they found no change in intensity during the sloping region but still assigned this region to sodium intercalation into graphene layers. This could be due to the poorer contrast between the atomic form factors of Na and C, in which case this should highlight the advantage of using SANS over SAXS for this type of investigation. More recently, Weaving *et al.* used *operando* Raman spectroscopy to show that the changes in the so-called "D" and "G" bands only occur during the sloping region and are unaffected during the plateau region.[30] As these bands are related to the carbon structure, they concluded that pore filling must be occurring in the plateau region as this did not impact the graphitic structure. Furthermore, our results are consistent with a recent molecular dynamics study[31] and a recent combined PDF and *operando* NMR study,[20] which both conclude that there are 3 regions, the first being due to surface processes, the second to intercalation and the third to pore-filling.

4 Conclusions

By conducting an *operando* SANS experiment, we have identified three distinct regions in the discharge profile of a hard-carbon-based sodium-ion battery, which we have assigned to different sodium-ion insertion processes. Our results provide direct supporting evidence for a 3-stage model, where the sodium is initially adsorbed onto the surface of particles (including SEI formation), then intercalated between the graphene layers, and finally inserted into the pores during the plateau region. These results contribute to the fundamental understanding of charge storage processes in this commercially relevant anode material which is essential in optimising its electrochemical properties.

More generally, these results demonstrate the capability of an *operando* SANS experiment to provide distinct information about the different sodium storage mechanisms in a nanoporous carbon material, and therefore address the characterisation challenges associated with this class of materials. The unique insights that this technique can provide make it a highly useful tool for understanding and optimising the electrochemical performance of new hard carbons. The limitations of this experiment mainly stemmed from the limited accessible Q-range of the instrument at PSI. Future experiments are planned using an instrument with a larger Q-range where information on the particle surface at low Q and the graphitic layer distances at high Q will also be accessible.

Data availability

The data collected and produced for this investigation are available upon reasonable request from the corresponding author.

Author contributions

E. M. R. and G. E. P. both conceived of and carried out the experiment, and prepared the manuscript; E. M. R. analysed the data; G. E. P. processed the data; J. F. carried out the experiment and prepared the manuscript; M. O. J., N. T.-R., H. Y. P., and S. H. supervised the project and edited the manuscript. I. M., S. A. C. and P. J. B. developed the electrochemical cell and provided it for use in this experiment.

Conflicts of interest

There are no conflicts to declare.

Acknowledgements

The Authors acknowledge the facilitators of the Materials Characterisation lab Gavin Stenning and Daniel Nye for the use of screening instruments, and SINQ for use of the SANS-I beamline at the PSI facility. The authors acknowledge the Faraday Institution for funding under the FIRG018 (Next Generation Na-ion batteries) and FIRG017 (FutureCat) projects.

Notes and references

1 X. Dou, I. Hasa, M. Hekmatfar, T. Diemant, R. J. Behm, D. Buchholz and S. Passerini, Pectin, Hemicellulose, or Lignin? Impact of the Biowaste Source on the Performance of Hard Carbons for Sodium-Ion Batteries, *ChemSusChem*, 2017, **10**(12), 2668–2676, DOI: 10.1002/cssc.201700628.

2 Z.-E. Yu, Y. Lyu, Y. Wang, S. Xu, H. Cheng, X. Mu, J. Chu, R. Chen, Y. Liu and B. Guo, Hard carbon micro-nano tubes derived from kapok fiber as anode materials for sodium-ion batteries and the sodium-ion storage mechanism, *Chem. Commun.*, 2020, **56**(5), 778–781, DOI: 10.1039/C9CC08221B.

3 M. Wahid, D. Puthusseri, Y. Gawli, N. Sharma and S. Ogale, Hard carbons for sodium-ion battery anodes: synthetic strategies, material properties, and storage mechanisms, *ChemSusChem*, 2018, **11**(3), 506–526, DOI: 10.1002/cssc.201701664.

4 X. Dou, I. Hasa, D. Saurel, C. Vaalma, L. Wu, D. Buchholz, D. Bresser, S. Komaba and S. Passerini, Hard carbons for sodium-ion batteries: Structure, analysis, sustainability, and electrochemistry, *Mater. Today*, 2019, **23**, 87–104, DOI: 10.1016/j.mattod.2018.12.040.

5 H. Marsh and F. Rodríguez-Reinoso, *Activated Carbon*, Elsevier, 2006.

6 Y. Liu, J. S. Xue, T. Zheng and J. R. Dahn, Mechanism of lithium insertion in hard carbons prepared by pyrolysis of epoxy resins, *Carbon*, 1996, **34**(2), 193–200, DOI: 10.1016/0008-6223(96)00177-7.

7 E. R. Bueil, A. George and J. R. Dahn, Model of micropore closure in hard carbon prepared from sucrose, *Carbon*, 1999, **37**(9), 1399–1407, DOI: 10.1016/S0008-6223(98)00335-2.

8 J. R. Dahn, W. Xing and Y. Gao, The "falling cards model" for the structure of microporous carbons, *Carbon*, 1997, **35**(6), 825–830, DOI: 10.1016/S0008-6223(97)00037-7.

9 F. Xie, Z. Xu, Z. Guo and M. M. Titirici, Hard carbons for sodium-ion batteries and beyond, *Prog. Energy*, 2020, **2**(4), 042002, DOI: 10.1088/2516-1083/aba5f5.

10 D. A. Stevens and J. R. Dahn, High capacity anode materials for rechargeable sodium-ion batteries, *J. Electrochem. Soc.*, 2000, **147**(4), 1271, DOI: 10.1149/1.1393348.

11 D. A. Stevens and J. R. Dahn, The mechanisms of lithium and sodium insertion in carbon materials, *J. Electrochem. Soc.*, 2001, **148**(8), A803, DOI: 10.1149/1.1379565.

12 D. A. Stevens and J. R. Dahn, An *in situ* small-angle X-ray scattering study of sodium insertion into a nanoporous carbon anode material within an operating electrochemical cell, *J. Electrochem. Soc.*, 2000, **147**(12), 4428, DOI: 10.1149/1.1394081.

13 S. Komaba, W. Murata, T. Ishikawa, N. Yabuuchi, T. Ozeki, T. Nakayama, A. Ogata, K. Gotoh and K. Fujiwara, Electrochemical Na insertion and solid electrolyte interphase for hard-carbon electrodes and application to Na-Ion batteries, *Adv. Funct. Mater.*, 2011, **21**(20), 3859–3867, DOI: 10.1002/adfm.201100854.

14 E. M. Lotfabad, P. Kalisvaart, A. Kohandehghan, D. Karpuzov and D. Mitlin, Origin of non-SEI related coulombic efficiency loss in carbons tested against Na and Li, *J. Mater. Chem. A*, 2014, **2**(46), 19685–19695, DOI: **10.1039/C4TA04995K**.

15 A. Gomez-Martin, J. Martinez-Fernandez, M. Ruttert, M. Winter, T. Placke and J. Ramirez-Rico, Correlation of Structure and Performance of Hard Carbons as Anodes for Sodium Ion Batteries, *Chem. Mater.*, 2019, **31**(18), 7288–7299, DOI: **10.1021/acs.chemmater.9b01768**.

16 N. Sun, Z. Guan, Y. Liu, Y. Cao, Q. Zhu, H. Liu, Z. Wang, P. Zhang and B. Xu, Extended "Adsorption–Insertion" Model: A New Insight into the Sodium Storage Mechanism of Hard Carbons, *Adv. Energy Mater.*, 2019, **9**(32), 1901351, DOI: **10.1002/aenm.201901351**.

17 S. Alvin, D. Yoon, C. Chandra, R. F. Susanti, W. Chang, C. Ryu and J. Kim, Extended flat voltage profile of hard carbon synthesized using a two-step carbonization approach as an anode in sodium ion batteries, *J. Power Sources*, 2019, **430**, 157–168, DOI: **10.1016/j.jpowsour.2019.05.013**.

18 B. Zhang, C. M. Ghimbeu, C. Laberty, C. Vix-Guterl, J.-M. Tarascon, B. Zhang, M. Tarascon, C. M. Ghimbeu, C. Laberty, C. Vix-Guterl and J.-M. Tarascon, Correlation Between Microstructure and Na Storage Behavior in Hard Carbon, *Adv. Energy Mater.*, 2015, **6**(1), 1501588, DOI: **10.1002/aenm.201501588**.

19 Y. Li, Y. Lu, Q. Meng, A. C. S. Jensen, Q. Zhang, Q. Zhang, Y. Tong, Y. Qi, L. Gu, M.-M. Titirici, Y.-S. Hu, Y. Q. Li, Y. X. Lu, Q. S. Meng, Q. Q. Zhang, Y. R. Qi, Y. s Hu, A. C. S. Jensen, Q. H. Zhang, Y. X. Tong, L. Gu and M. m Titirici, Regulating Pore Structure of Hierarchical Porous Waste Cork-Derived Hard Carbon Anode for Enhanced Na Storage Performance, *Adv. Energy Mater.*, 2019, **9**(48), 1902852, DOI: **10.1002/aenm.201902852**.

20 J. M. Stratford, A. K. Kleppe, D. S. Keeble, P. A. Chater, S. Meysami, C. J. Wright, J. Barker, M.-M. Titirici, P. K. Allan and C. P. Grey, Correlating Local Structure and Sodium Storage in Hard Carbon Anodes: Insights from Pair Distribution Function Analysis and Solid-State NMR, *J. Am. Chem. Soc.*, 2021, **143**(35), 14274–14286, DOI: **10.1021/jacs.1c06058**.

21 X. Chen, C. Liu, Y. Fang, X. Ai, F. Zhong, H. Yang and Y. Cao, Understanding of the sodium storage mechanism in hard carbon anodes, *Carbon Energy*, 2022, **4**(6), 1133–1150, DOI: **10.1002/cey2.196**.

22 C. A. Bridges, X.-G. Sun, J. Zhao, M. P. Paranthaman and S. Dai, *In Situ* Observation of Solid Electrolyte Interphase Formation in Ordered Mesoporous Hard Carbon by Small-Angle Neutron Scattering, *J. Phys. Chem. C*, 2012, **116**(14), 7701–7711, DOI: **10.1021/jp3012393**.

23 S. Risse, E. Härk, B. Kent and M. Ballauff, *Operando* Analysis of a Lithium/Sulfur Battery by Small-Angle Neutron Scattering, *ACS Nano*, 2019, **13**(9), 0233–10241, DOI: **10.1021/acsnano.9b03453**.

24 D. Saurel, J. Segalini, M. Jauregui, A. Pendashteh, B. Daffos, P. Simon and M. Casas-Cabanas, A SAXS outlook on disordered carbonaceous materials for electrochemical energy storage, *Energy Storage Mater.*, 2019, **21**, 162–173, DOI: **10.1016/j.ensm.2019.05.007**.

25 K. C. Ltd, *Anode Material for Lithium-Ion Battery KURANODE™ BIOHARDCARBON*, 2023.

26 I. Mcclelland, S. G. Booth, N. N. Anthonisamy, L. A. Middlemiss, G. E. Pérez, E. J. Cussen, P. J. Baker and S. A. Cussen, Direct Observation of Dynamic Lithium Diffusion Behavior in Nickel-Rich, $LiNi_{0.8}Mn_{0.1}Co_{0.1}O_2$ (NMC811) Cathodes Using *Operando* Muon Spectroscopy, *Chem. Mater.*, 2023, **35**(11), 4149–4158, DOI: **10.1021/acs.chemmater.2c03834**.

27 P. S. Institut, *SINQ: The Swiss Spallation Neutron Source*, 2023.

28 M. A. Reddy, M. Helen, A. Groß, M. Fichtner and H. Euchner, Insight into Sodium Insertion and the Storage Mechanism in Hard Carbon, *ACS Energy Lett.*, 2018, **3**(12), 2851–2857, DOI: **10.1021/acsenergylett.8b01761**.

29 H. Alptekin, H. Au, A. C. Jensen, E. Olsson, M. Goktas, T. F. Headen, P. Adelhelm, Q. Cai, A. J. Drew and M.-M. Titirici, Sodium Storage Mechanism Investigations through Structural Changes in Hard Carbons, *ACS Appl. Energy Mater.*, 2020, **3**(10), 9918–9927, DOI: **10.1021/acsaem.0c01614**.

30 J. S. Weaving, A. Lim, J. Millichamp, T. P. Neville, D. Ledwoch, E. Kendrick, P. F. Mcmillan, P. R. Shearing, C. A. Howard and D. J. L. Brett, Elucidating the Sodiation Mechanism in Hard Carbon by *Operando* Raman Spectroscopy, *ACS Appl. Energy Mater.*, 2020, **3**(8), 7474–7484, DOI: **10.1021/acsaem.0c00867**.

31 J. Li, C. Peng, J. Li, J. Wang and H. Zhang, Insight into Sodium Storage Behaviors in Hard Carbon by ReaxFF Molecular Dynamics Simulation, *Energy Fuels*, 2022, **36**(11), 5937–5952, DOI: **10.1021/acs.energyfuels.2c00575**.